American Journal of Chemical and Biochemical Engineering
2026, Vol. 10, No. 1, pp. 1–21
https://doi.org/10.11648/j.ajcbe.20261001.11

Research Article

Molecular Modelling Applied to the Computer-aided Design of Inhibitors of Mycobacterium Tuberculosis Aminoglycoside Acetyltransferase (Eis) to Combat Kanamycin Resistance

Bamba Ibrahim[1], Kouadja Rika Justin[1], Mousse Logbo Mathias[1], Soro Issouf[1], Niare Adama[1, *], Megnassan Eugene[1, 2, 3]

[1]Laboratory of Fundamental and Applied Physics, Nangui Abrogoua University, Abidjan, Côte d'Ivoire

[2]Laboratory of Crystallography and Molecular Physics, Felix Houphouët-BOIGNY University, Abidjan, Côte d'Ivoire

[3]Quantitative Life Sciences (QLS), Abdus Salam International Centre for Theoretical Physics (ICTP-UNESCO), Trieste, Italy

Abstract

Globally, tuberculosis continues to be a primary cause of death resulting from infectious diseases. The rise of resistant bacterial strains significantly undermines the effectiveness of current treatments. This study examines new sulfonamide derivatives (SULF) that target the Eis enzyme of Mycobacterium tuberculosis. This enzyme plays a direct role in kanamycin resistance. Three-dimensional models of the Eis-SULF complexes were generated from the reference crystal structure (PDB: 5IV0). These complexes were used to construct a test set of thirteen compounds with known experimental activities and an external validation set of four additional compounds. Active conformations were identified using energy-based QSAR modeling. The gas-phase model exhibits an R^2 coefficient of 0.96. Cross-validation of the gas-phase model yields an R^2_{cv} value of 0.95. The standard error of the gas-phase model is 0.28. The model in a solvated environment shows an R^2 value of 0.97. Cross-validation in a solvated environment yields an R^2_{cv} of 0.96. The standard error in a solvated environment is 0.24. A virtual library of sulfonamides was then constructed. The screening was based on Lipinski's rules and the PH4 model. The PH4 model has an R^2 value of 0.91. The standard error of the PH4 model is 0.45. Sixty-five compounds show potential for oral bioavailability. The most promising complexes were studied using molecular dynamics. This analysis assesses the stability of ligands in the active site. The MM/GBSA approach was employed to calculate the binding free energies of the complexes. These calculations confirm a high affinity for the Eis enzyme. This integrated approach proposes promising new inhibitors against drug-resistant tuberculosis.

Keywords

Drug-resistant Tuberculosis, Eis Enzyme, Sulfonamide, Molecular Modeling, QSAR, Molecular Dynamics, MM/GBSA

*Correspondence: Niare Adama (niareadamabonheur@gmail.com)

Received: 8 May 2026; **Accepted:** 19 May 2026; **Published:** 30 May 2026

1. Introduction

Globally, tuberculosis persists as a principal cause of mortality due to infectious agents. In its 2025 report, the World Health Organization documented over 10.7 million incident cases and approximately 1.2 million fatalities for the year 2024 [1]. Despite medical advances, the disease remains difficult to control. This critical health crisis is further compounded by the continuous propagation of multidrug-resistant (MDR) and extensively drug-resistant (XDR) bacterial variants. These resistant forms threaten current treatment strategies and reduce the effectiveness of conventional aminoglycoside-based therapies. Second-line medications are also heavily affected [2, 3]. A better understanding of resistance mechanisms is therefore necessary. This knowledge is essential for developing new therapeutic approaches. Among these mechanisms, the Eis (Enhanced Intracellular Survival) enzyme plays a central role. This enzyme belongs to the aminoglycoside acetyltransferase family. Eis inactivates several aminoglycosides through a process of acetylation. Studies have shown its action on kanamycin and amikacin. Capreomycin is also affected by this enzymatic inactivation [4, 5]. Overexpression of Eis promotes clinical resistance to kanamycin. This resistance leads to therapeutic failures in MDR TB patients [6]. Eis also plays a role in the intracellular survival of the bacterium. This enzyme influences cellular mechanisms in the infected host. In particular, it modifies autophagy and the inflammatory response [7]. These functions reinforce the interest of Eis as a priority therapeutic target. The catalytic site of Eis has a predominantly hydrophobic cavity. This cavity is organized around conserved aromatic residues. These residues participate in ligand recognition. They also stabilize inhibitory enzyme complexes [8, 9]. Structural studies confirm their role in ligand binding. Bulky aromatic groups are strongly favored. Hydrophobic molecules thus show an increased affinity for Eis [10]. This organization makes sulfonamides particularly interesting. These compounds possess good chemical stability. They exhibit great structural diversity. They interact effectively with biological hydrophobic pockets [11].

Computer-aided design has transformed drug discovery. It allows for the rapid exploration of large virtual libraries. Structural modeling plays a central role in these approaches. QSAR methods facilitate the analysis of structure-activity relationships. Virtual screening reduces initial experimental costs [12, 13]. Furthermore, molecular dynamics simulations are implemented to assess the structural integrity of the generated complexes and to monitor the conformational fluctuations occurring within the catalytic pocket. MM/GBSA calculations more accurately estimate binding energies [14, 15]. New antituberculosis drugs have improved certain treatments. Bedaquiline and pretomanid are recent examples. Delamanid has also shown clinical efficacy. However, treatment failures still persist today. The bacterium adapts rapidly to new drug pressures [16]. In this context, targeting Eis remains a relevant complementary option. Among known Eis inhibitors, compound 46 is particularly active (Figure 1). This activity is linked to a specific naphthyl group. This group inserts deeply into the hydrophobic cavity [17]. Despite these results, few structures have been explored. Significant optimization potential therefore remains available. This study is based on the Eis sulfonamide code pdb: 5IV0 crystal structure [17]. In situ modifications allowed the generation of several complexes. Complexation energies were calculated for each ligand. These values were used to build reliable QSAR models. A three-dimensional PH4 pharmacophore model was then established. This model identifies the essential characteristics for inhibition. A large virtual library of sulfonamides was screened. The strategy also includes molecular dynamics simulations. MM/GBSA calculations complement the energetic analysis of the complexes. The objective is to identify new, more efficient inhibitors. These compounds could contribute to the treatment of resistant tuberculosis.

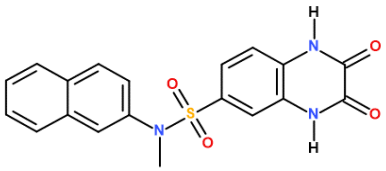

Figure 1. *Structure of compound 46.*

2. Methods

2.1. Training and Validation Sets

In vitro bioactivity metrics targeting the Eis protein were retrieved from a specific, previously published experimental investigation [17]. The values cover a sufficiently wide range (0,24 nM $\leq$ $IC_{50}^{exp} \leq$ 2700 nM) for reliable modeling. This variability facilitates the establishment of robust structure-activity relationships. Thirteen (13) sulfonamide inhibitors were selected as the test set (TS). Four (4) additional compounds constituted the external validation set (VS). The distribution of the compounds complies with OECD recommendations [18].

2.2. Model Building

The crystallographic coordinates of the Eis protein (PDB ID: 5IV0) [17] served as the primary template. The intrinsic covalent bond was computationally removed. The step facilitated the evaluation of non-covalent binding within the catalytic pocket. Subsequent modeling and structural preparations utilized Insight II [19] and Discovery Studio [20], following validated computational protocols [21].

2.3. Molecular Mechanics

Molecular mechanics was used to describe the systems studied. Isolated inhibitors were represented by a complete atomic model. Enzyme-ligand complexes were treated according to established procedures [22-24]. Interatomic interactions were described using the CFF force field [25]. The structures were subjected to unconstrained energy minimization.

2.4. Conformational Research

Free inhibitor conformations were generated through complete energy relaxation. This followed a comprehensive conformational sampling. Internal rotations were sampled using a Monte Carlo approach, yielding two hundred distinct conformers per inhibitor. The lowest-energy conformer was retained for subsequent local optimization, performed with a dielectric constant set to 4. Computational parameters aligned with prior studies [26].

2.5. Gibbs Free Energies Solvation

Solvation free energies were calculated using the DelPhi module [20]. Non-linear Poisson-Boltzmann equation were solved to evaluate the electrostatic component [27]. The calculations were performed on a high-resolution three-dimensional grid, with the ionic strength fixed at a physiological value. The resulting free energy corresponds to the reaction field energy [28]. All numerical parameters and calculation protocols are consistent with previously reported methods [24, 29].

2.6. Calculation of the Entropic Term

Entropy changes upon complexation were assessed. contribution was evaluated during complex formation. This estimate is based on a simplified approach reported previously [30, 31]. The normal modes of vibration of the inhibitors were analyzed [32]. Conformational entropy reflects the flexibility of the ligand. Free ligands were compared to ligands bound to the active site.

2.7. Calculation of Binding Affinity and QSAR Model

Binding affinity computations via GFE followed established protocols [21].

2.8. Interaction Energy

CFF force field applications calculated the enzyme-inhibitor the interaction energies (E_{int}), as previously described [21].

2.9. Generation of Pharmacophores

Discovery Studio [20] generated the 3D-QSAR (PH4) pharmacophore. This process utilized the Catalyst HypoGen algorithm to model Eis inhibition [27].

2.10. ADME Properties

QikProp [33] estimated the pharmacokinetic profiles, following standard procedures [27].

2.11. Virtual library Generation

Virtual library construction followed reference [14].

2.12. ADME Based Library

Selection criteria filtered the virtual library. These included geometric constraints, molecular alignment, and interaction patterns [24, 27].

2.13. Pharmacophore-based Library Search

The PH4 model screened the library [27]. This model originated from SULF bound conformations within the Eis catalytic pocket.

2.14. Inhibitory Power Prediction

Within each subset group, the conformer optimally aligned to the PH4 model was chosen for in silico screening using the complexation QSAR model. The $\Delta\Delta G_{com}$ value of each newly selected analog was evaluated to estimate its Eis inhibitory potency (pIC_{50}^{pre}). This prediction was incorporated into the target-specific scoring function, specified in equation 1, which was parameterized using the SULF inhibitor training set from the complexation QSAR model [17].

$$pIC_{50}^{exp} = -\log_{10} IC_{50}^{exp} = a.\Delta\Delta G_{com} + b \quad (1)$$

2.15. Molecular Dynamics Simulations

Molecular dynamics simulations assessed complex stability. This approach studies structural evolution over time. The simulations were performed using Desmond software [34]. This program is suitable for large biomolecular systems [36]. The protocols applied are described in previous studies [35].

2.16. GB/SA Binding Free Energy Calculations

MM/GBSA methodologies calculated the binding free energies. This approach combines molecular mechanics and implicit solvation [36]. The calculations are based on trajectories derived from molecular dynamics. Each enzyme-ligand complex was analyzed independently. Average energy contributions were extracted from representative structures. The values obtained allow the relative stability of the complexes to be compared.

3. Results

Seventeen SULF derivatives (Table 1) were selected. Their experimental properties were previously determined by a single laboratory [17]. The reported inhibitory activity (0.24 nM $\leq IC_{50}^{exp} \leq$ 27,000 nM) [17] encompass a large concentration range, allowing the establishment of a robust QSAR model. The ratio of training and validation set sizes is critical for robust classification. However, limited homologous datasets constrain this step [37]. In this work, a training set of 13 SULFs and a validation set of 4 SULFs were partitioned using Discovery Studio 2.5 [20].

Table 1. *Chemical structures of the 17 Eis inhibitors employed to construct the QSAR binding model [17].*

Training set		
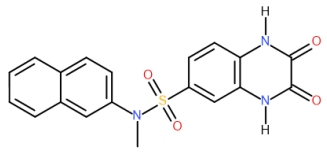	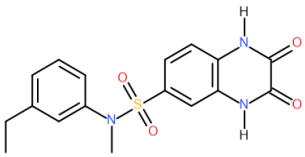	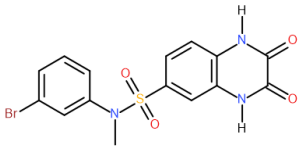
SULF1 ($IC_{50}^{exp} = 0{,}24$ nM)	SULF2 ($IC_{50}^{exp} = 27$ nM)	SULF3 ($IC_{50}^{exp} = 56$ nM)
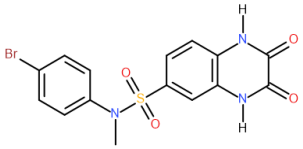	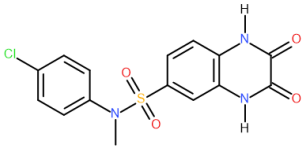	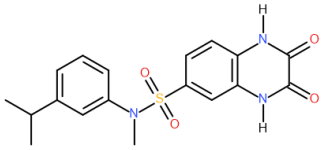
SULF4 ($IC_{50}^{exp} = 80$ nM)	SULF5 ($IC_{50}^{exp} = 100$ nM)	SULF6 ($IC_{50}^{exp} = 230$ nM)
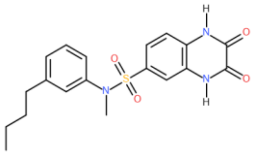	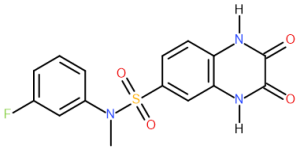	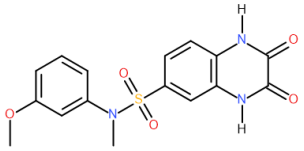
SULF7 ($IC_{50}^{exp} = 700$ nM)	SULF8 ($IC_{50}^{exp} = 3000$ nM)	SULF9 ($IC_{50}^{exp} = 5800$ nM)
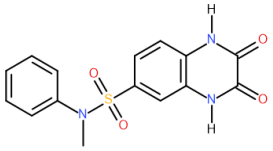	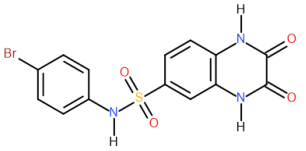	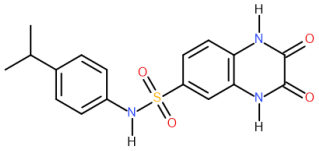
SULF10 ($IC_{50}^{exp} = 5800$ nM)	SULF11 ($IC_{50}^{exp} = 6200$ nM)	SULF12 ($IC_{50}^{exp} = 10600$ nM)
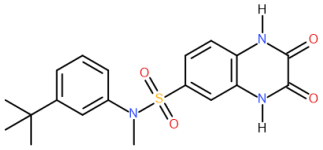		
SULF13 ($IC_{50}^{exp} = 27000$ nM)		
Validation Set		
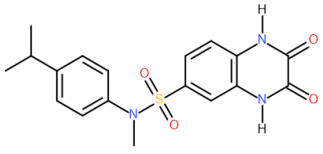	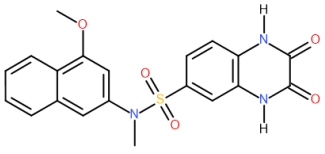	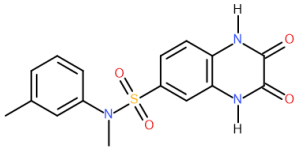
SULF1 ($IC_{50}^{exp} = 250$ nM)	SULF2 ($IC_{50}^{exp} = 300$ nM)	SULF3 ($IC_{50}^{exp} = 370$ nM)

Training set

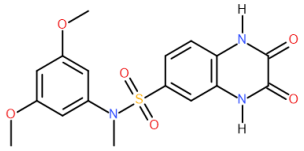

SULF4 ($IC_{50}^{exp} = 7400$ nM

3.1. QSAR Model

One-descriptor QSAR model: Thirteen TS and four VS complexes were generated via in situ modification of the refined 5IV0 crystal structure [17]. Methodological details are provided above. For all seventeen optimized complexes, the relative Gibbs free energy of binding ($\Delta\Delta G_{com}$) was evaluated. The resulting $\Delta\Delta G_{com}$ components for both sets are detailed in Table 2. To construct the QSAR model, experimental inhibitory activities (IC_{50}^{exp}) were converted to pIC_{50}^{exp}. These values were then linearly regressed against the computed $\Delta\Delta G_{com}$ (Table 2). This strong correlation confirmed the functional binding poses of the ligands, facilitating the derivation of the PH4 pharmacophore. Gas-phase complexation enthalpy ($\Delta\Delta H_{MM}$) was also assessed against pIC_{50}^{exp} to elucidate binding affinities. As shown in Table 3, this linear relationship underscores the critical role of direct enzyme-inhibitor contacts. This is particularly evident when desolvation and entropic penalties are excluded. Enthalpic factors alone explained 96% of the experimental variance. Further analysis incorporated the complete GFE terms ($\Delta\Delta H_{MM}$, $\Delta\Delta TS_{vib}$, and $\Delta\Delta G_{sol}$), detailed in Table 3. The robust R ²values confirm that these 3D-derived insights reliably forecast the activity of new SULF derivatives sharing this binding paradigm.

Binding mode of SULFs: The investigated SULF compounds belong to a previously reported class of sulfonamides [17]. These molecules are recognized for chelating metal ions. Their acidic moiety plays a crucial role in suppressing Eis activity. Structural analysis relied on the 5IV0 crystal data, specifically the Eis-SULF1 co-complex. This structure demonstrates ligand accommodation within the aminoglycoside cavity. Hydrophobic contacts and π–π stacking primarily drive this stabilization.

Interaction Energy: Interaction energy (IE, ΔE_{int}) profiles were constructed for all TS molecules to extract structural determinants. Residue-specific IE decomposition highlighted potential sites for R-group optimization. Targeting these regions could enhance overall affinity and potency. We categorized the inhibitors by activity level (high, moderate, low) to compare their IE patterns (Figure 4). This permitted a detailed evaluation of individual amino acid contributions. Nevertheless, the analysis revealed uniform residue-level IE profiles across all activity tiers. Consequently, no obvious pathways for advantageous chemical substitutions were identified.

Table 2. *Computed binding affinities (Gibbs free energy) and thermodynamic components for the training (SULF1-13) and validation (SULF1-4) sets [17].*

Training set-New id.	Old id. [17]	IC_{50}^{exp} (nM)	M_w [g.mol^{-1}]	$\Delta\Delta H_{MM}$ [kcal.mol^{-1}]	$\Delta\Delta G_{sol}$ [kcal.mol^{-1}]	$\Delta\Delta TS_{vib}$ [kcal.mol^{-1}]	$\Delta\Delta G_{com}$ [kcal.mol^{-1}]	pIC_{50}^{exp}
SULF1	46	0,24	381	0.00	0.00	0.00	0.00	9.62
SULF2	42	27	359	12.45	-0.97	1.74	9.73	7.57
SULF3	38	56	410	15.89	-3.32	1.28	11.29	7.25
SULF4	29	80	410	16.97	-3.43	0.84	12.70	7.10
SULF5	35	100	366	17.25	-3.55	1.21	12.49	7.00
SULF6	43	230	373	21.61	1.48	4.58	18.52	6.64
SULF7	44	700	387	22.70	0.61	6.47	16.84	6.15
SULF8	37	3000	349	23.55	1.87	3.24	22.18	5.52
SULF9	39	5800	361	25.11	-0.12	2.92	22.07	5.24
SULF10	31	5800	331	24.69	2.30	4.39	22.60	5.24

Training set-New id.	Old id. [17]	IC_{50}^{exp} (nM)	M_w [g.mol^{-1}]	$\Delta\Delta H_{MM}$ [kcal.mol^{-1}]	$\Delta\Delta G_{sol}$ [kcal.mol^{-1}]	$\Delta\Delta TS_{vib}$ [kcal.mol^{-1}]	$\Delta\Delta G_{com}$ [kcal.mol^{-1}]	pIC_{50}^{exp}
SULF11	30	6200	396	25.04	-3.95	0.25	20.84	5.21
SULF12	34	10600	359	26.06	2.01	3.81	24.26	4.97
SULF13	45	27000	387	30.59	-0.37	4.54	25.68	4.57

Validation Set New id.	Old id. [17]	IC_{50}^{exp} (nM)	pIC_{50}^{exp}	M_W [g.mol^{-1}]	$\Delta\Delta H_{MM}$ [kcal.mol^{-1}]	$\Delta\Delta G_{sol}$ [kcal.mol^{-1}]	$\Delta\Delta TS_{vib}$ [kcal.mol^{-1}]	$\Delta\Delta G_{com}$ [kcal.mol^{-1}]	pIC_{50}^{pre}	pIC_{50}^{pre}/ pIc_{50}^{exp}
SULF1	33	250	6.60	373	16.89	2.69	5.13	14.45	6.77	1.03
SULF2	47	250	6.52	411	17.09	1.27	0.75	17.61	6.17	0.95
SULF3	41	370	6.43	345	20.25	2.10	3.06	19.29	5.85	0.91
SULF4	40	7400	5.13	391	23.08	0.16	1.58	21.65	5.41	1.05

Table 3. *Evaluation of calculated binding affinities ($\Delta\Delta G_{com}$), the corresponding enthalpic term ($\Delta\Delta H_{MM}$), and empiric inhibitory metric $pIC_{50}^{exp} = -log_{10}IC_{50}^{exp}$ for SULF derivates against the Eis protein [17].*

Statistical Data of Linear Regression	(A)	(B)
$pIC_{50}^{exp} = -0.1756 \times \Delta\Delta H_{MM} + 9.8522$ $pIC_{50}^{exp} = -0.189 \times \Delta\Delta G_{com} + 9.5001$		
Number of compounds n	13	13
Squared correlation coefficient of regression R^2	0.96	0.97
LOO cross-validated squared correlation coefficient R_{cv}^2	0.95	0.96
Standard error of regression σ	0.28	0.24
Statistical significance of regression, Fisher F-test	270.55	371.64
Level of statistical significance α	> 95%	> 95%
Range of activities IC_{50}^{exp}(nM) [17]	0.24 - 27000	

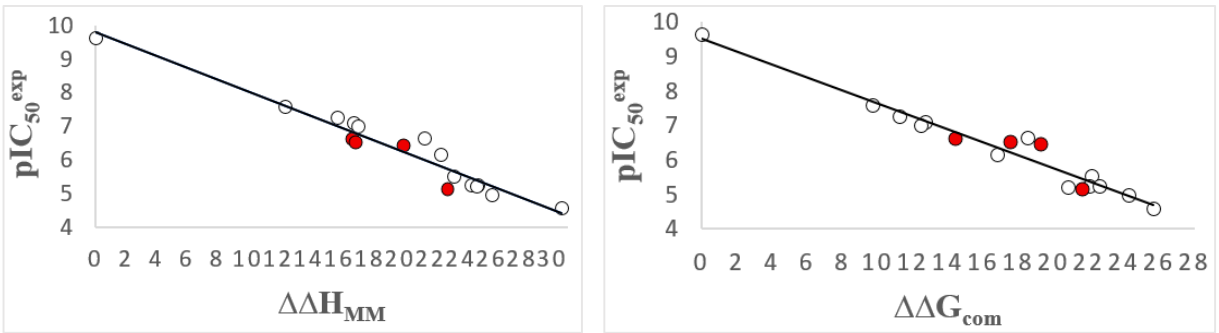

Figure 2. *(Left) Linear regression analysis comparing the empirical pIC_{50}^{exp} values against the computed enthalpic term ($\Delta\Delta H_{MM}$ [kcal.mol^{-1}]), (Right) An equivalent graphical representation illustrating the relationship with the total complexation Gibbs free energy ($\Delta\Delta G_{com}$ [kcal.mol^{-1}]) for the training molecules [17], Red markers identify the validation set compounds.*

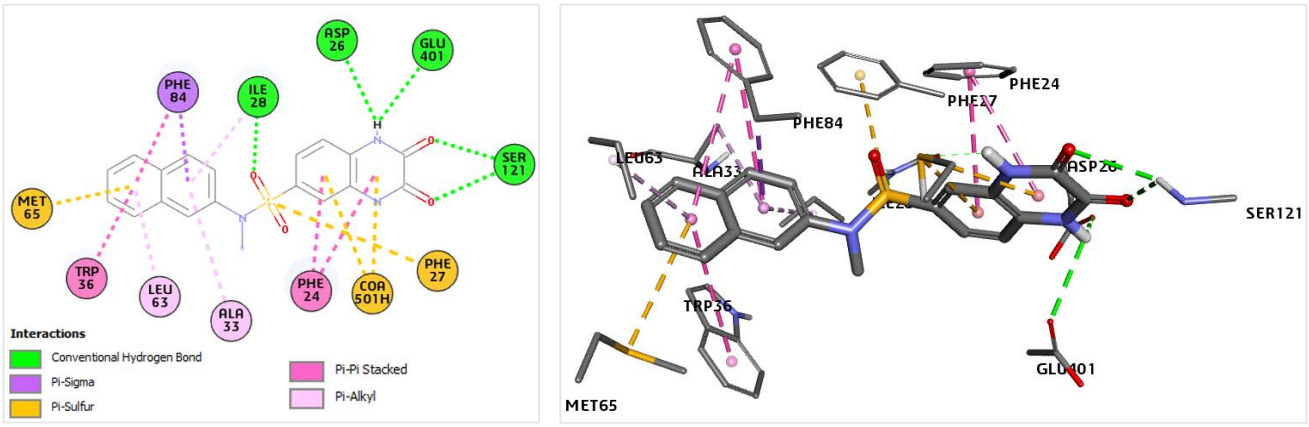

Figure 3. *(Left) Two-dimensional representation mapping the binding interactions of the highly active SULF1 molecule within the Eis catalytic pocket. (Right) Three-dimensional visualization detailing the same enzyme-ligand spatial arrangement.*

Figure 4. *Per-residue decomposition of the intermolecular interaction energies (E_{int}) derived from molecular mechanics computations (values in kcal mol^{-1}). The charts group the derivatives by potency: (top) highly active compounds; (center) intermediate activity analogs; and (bottom) low activity variants (Table 2 [4]).*

3.2. 3D-QSAR Pharmacophore Model

Generation and validation of the 3D-QSAR pharmacophore: To inhibit the Eis enzyme, a predictive 3D-pharmacophore framework was constructed utilizing the active geometries of the thirteen TS compounds. Subsequent validation employed the four VS molecules. These compounds cover a wide range of experimental activities (0.24-27,000 nM), spanning approximately three orders of magnitude. As detailed in prior work [32], the generation workflow progressed through three distinct phases: construction, subtraction, and final optimization [38].

Candidate hypotheses underwent rigorous evaluation concerning complexity, statistical robustness, and predictive accuracy. We retained the top ten distinct models, all possessing five key pharmacophoric features. Table 4 lists all of these hypotheses' statistical parameters. Selection criteria prioritized minimal RMSD, reduced overall cost, and strong correlation coefficients. By subtracting the fixed cost (29.9) from the null cost (2557.2), a substantial cost difference (Δ = 2527.3) was determined. This wide margin guarantees a statistical confidence exceeding 90% for a genuine correlation [39]. Hypothesis 1 (Hypo1) was further assessed by aligning it with SULF1, the most potent TS derivative. Figure 5D visualizes this ideal binding geometry for targeted Eis suppression. The predictive capacity of Hypo1 is defined by the regression formula $pIC_{50}^{exp} = 1{,}014 \times pIC_{50}^{pre} - 0{,}0916$. Plotted in Figure 5E, this linear relationship demonstrates excellent statistical metrics (n = 13, R^2= 0.91, R^2_{cv} = 0.90, F-test = 105.26, σ = 0.45, α > 95%). Consequently, this robust PH4 framework provides a dependable tool for discovering novel sulfonamide-based inhibitors.

Table 4. *Statistical parameters characterizing the ten optimal PH4 hypotheses targeting the Eis enzyme, including Cat-Scramble validation metrics (derived from 49 randomizations per model at a 98% confidence threshold).*

Hypothesis	RSMD [a]	R^2 [b]	Total Cost [c]	Costs Difference [d]	Closest Random [e]	Features [f]
Hypo 1	6.085	0.95	307.1	2250.1	354.17	HBA, HBD, HYD, HYD, HYD
Hypo 2	6.260	0.94	323.2	2234.0	414.84	HBA, HBD, HYD, HYD, HYD
Hypo 3	8.067	0.91	482.9	2074.3	468.24	HBA, HBD, HYD, HYD
Hypo 4	8.332	0.90	497.2	2060.0	495.72	HBA, HBD, HYD, HYD, HYD
Hypo 5	8.458	0.90	505.1	2052.1	618.78	HBA, HBD, HYD, HYD, HYD
Hypo 6	8.514	0.90	522.0	2035.2	644.83	HBA, HBD, HYD, HYD
Hypo 7	8.733	0.89	548,0	2009.2	647.29	HBD, HYD, HYD, HYD
Hypo 8	8,723	0,89	556.8	2000.4	661.16	HBA, HYD, HYD, HYD
Hypo 9	8.797	0,89	559.5	1997.7	661.79	HBA, HBD, HYD, HYD, HYD
Hypo 10	9.105	0.88	582.1	1975.1	674.17	HBA, HBD, HYD, HYD, HYD
Fixed Cost	0	0	29.9			
Null Cost	19.763	0	2557.2			

Configuration cost = 10.39.

[a] Root mean-squared deviation; [b] Squared correlation coefficient; [c] Total cost value for the PH4 pharmacophore; [d] Difference in cost between the hypothesis and the Null model; [e] Minimum cost derived from 49 scrambling iterations evaluated at a 98% confidence threshold. [f] Feature definitions: HBA (hydrogen-bond acceptor); HYD (hydrophobic); HBD (hydrogen-bond donor).

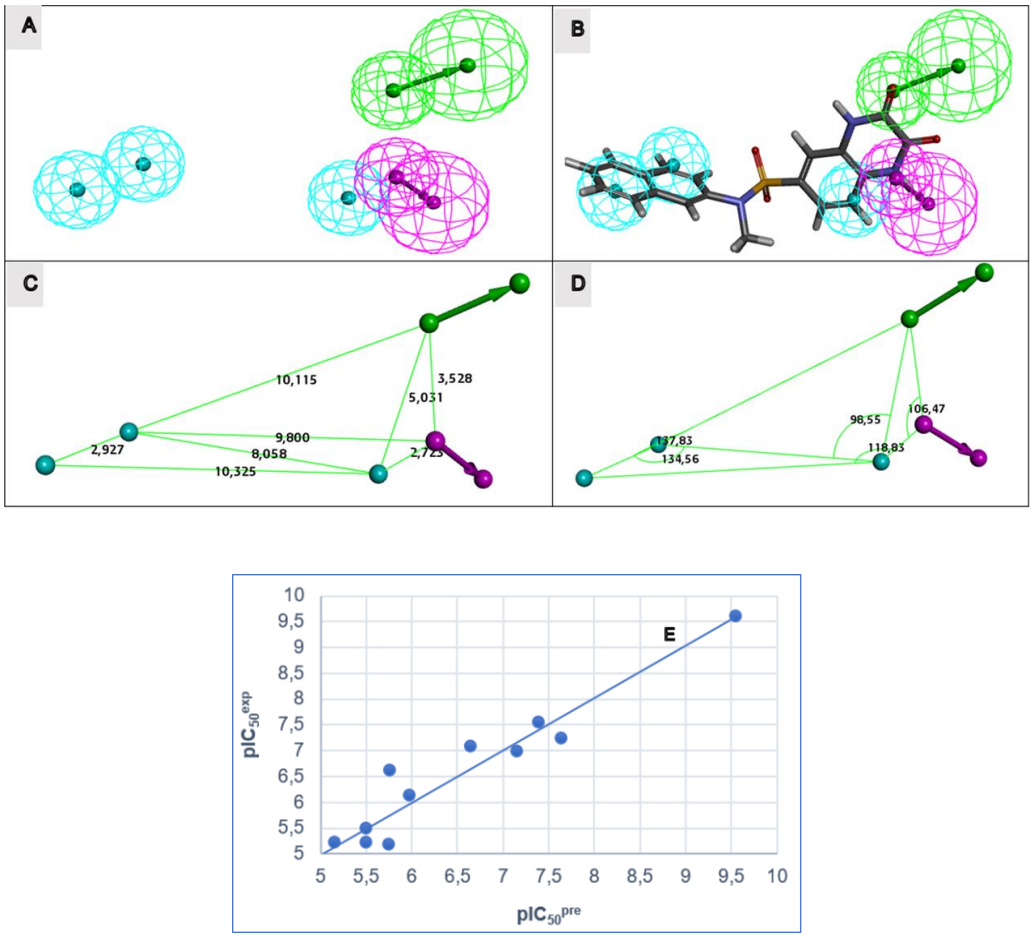

Figure 5. *(A) Spatial arrangement of the generated features. (B) Superimposition of the optimal pharmacophore onto SULF1, the highest-affinity Eis inhibitor. (C) Distances between centers, (D) angles between centers of pharmacophoric features. Feature legend: HYD = Hydrophobic (cyan), HBA = Hydrogen bond Acceptor (green), HBD = Hydrogen bond Donor (pink), Excluded volume. (E) Correlation plot of experimental vs. predicted inhibitory activity.*

3.3. Virtual Combinatorial Library of SULFs and in Silico Screening

Combinatorial library virtual screening has become a potent method for finding possible hit chemicals. Through the exploration of large chemical spaces and the prediction of important molecular interactions, our earlier research on inhibitor design has shown its efficacy in choosing potential candidates [40-42].

Virtual Library: To generate a comprehensive virtual library (VL), structural modifications were introduced at the R1 and R2 sites of the core SULF framework (Table 5). This systematic enumeration process yielded a vast collection of 51,800 distinct derivatives (calculated as 70 R_1 substituents × 740 R_2 substituents). During the assembly of these novel analogs, the specific substitution architecture characteristic of the most potent molecule, SULF1, was deliberately maintained.

This library was built using pieces taken from chemical databases of accessible substances [43]. To refine the dataset and ensure optimal pharmacokinetic profiles, several strict filtering criteria were applied. Notably, adherence to Lipinski's Rule of Five was mandatory; consequently, molecules exceeding the 500 g/mol molecular weight threshold were discarded [44]. This filtration step successfully condensed the initial dataset into a focused, high-quality collection perfectly suited for subsequent computational evaluations.

In silico Screening of Library of SULFs: To identify promising candidates, the curated dataset of 51,800 derivatives was computationally screened against the optimized Hypo1 pharmacophore targeting the Eis active site. A total of 65 novel structures successfully mapped onto a minimum of four essential PH4 features. These prime candidates (PH4 hits) subsequently underwent evaluation via the established complexation QSAR framework. The thermodynamic parameters resulting from this analysis-including the total Gibbs free energy (GFE) of binding and its individual components-are compiled in Table 6. Additionally, this table presents the predicted inhibitory potencies (pIC_{50}^{pred}), derived directly from the application of correlation Equation B (previously detailed in Table 3).

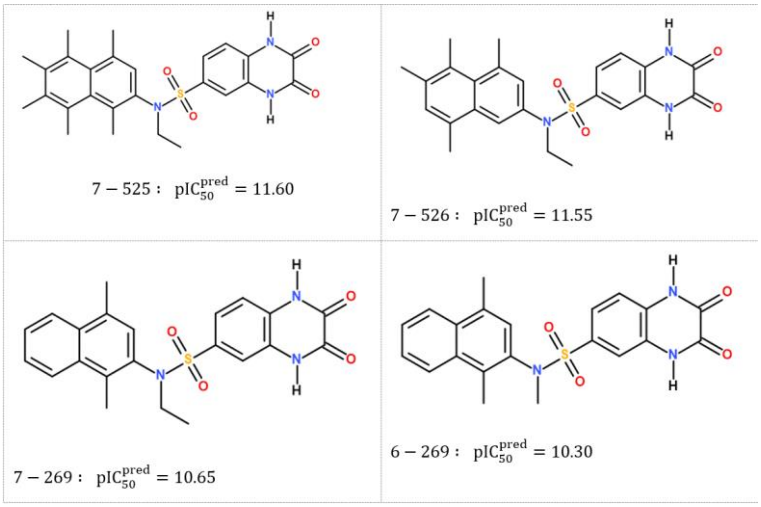

Figure 6. *Chemical structures and predicted activities (pIC_{50}^{pred}) of the most promising in silico designed SULF analogs.*

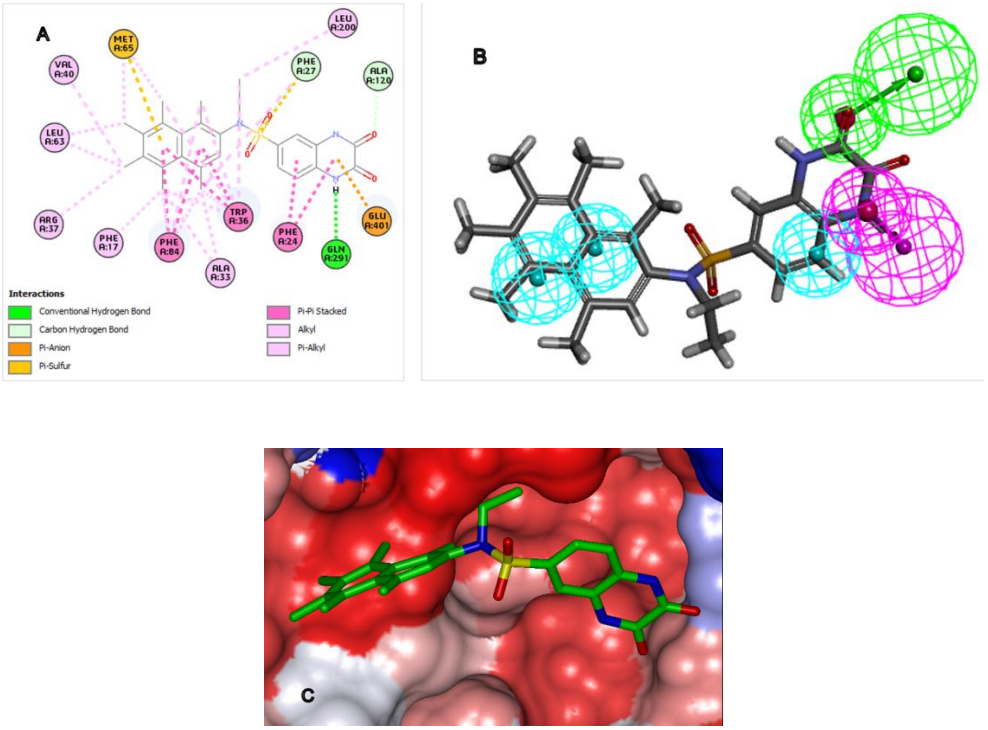

Figure 7. *(A) Two-dimensional interaction map illustrating the optimal designed candidate, SULF 7-525, docked within the Eis catalytic pocket. (B) Spatial alignment of the SULF 7-525 derivative against the established PH4 inhibitory model. (C) Three-dimensional representation of the Eis active site's Connolly surface accommodating the reference SULF 7-525 structure. (Color scheme: hydrophobic regions in red, hydrophilic areas in blue, and intermediate zones in white).*

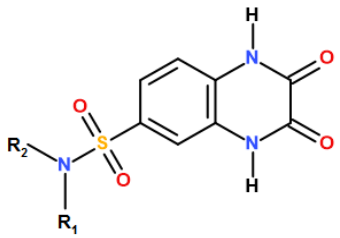

Figure 8. *Core chemical scaffold of the sulfonamide (SULF) library illustrating the R_1 and R_2 substitution positions.*

Table 5. *Inventory of the R-group fragments utilized for generating the computational SULF library. For the 65 highest-ranking candidates, total binding free energies (GFE) and their corresponding thermodynamic components were evaluated. The nomenclature for these novel analogs is derived by concatenating the specific R_1 and R_2 substituent identifiers established in this table.*

Designed analogs	Substituents		M_w [g.mol^{-1}]	$\Delta\Delta H_{MM}$ [kca.mol^{-1}]	$\Delta\Delta G_{sol}$ [kca.mol^{-1}]	$\Delta\Delta TS_{vib}$ [kca.mol^{-1}]	$\Delta\Delta G_{com}$ [kca.mol^{-1}]	pIC_{50}^{pred}
	R_1	R_2						
SULF1	CH_3	naphtalen-2-yl	381	0.00	0.00	0.00	0.00	9.62*
1-239	H	3-bromonaphtalen-2-yl	446	13.23	1.05	0.90	13.38	6.67
1-444	H	6-bromo-2H-chromen-7-yl	450	1.32	0.64	2.30	-0.34	9.56
1-450	H	6-hydroxy-2*H*-chromen-7-yl	401	-0.11	0.83	3.12	-2.39	9.95
2-84	F	2-chloro-5-methoxyphenyl	400	3.09	0.97	4.79	-0.73	9.64
2-113	F	3-ethoxyphenyl	379	3.36	0.22	3.43	0.15	9.47
2-234	F	4-methoxynaphthalen-2-yl	415	6.07	2.51	1.97	6.62	8.25
2-240	F	1-bromonaphthalen-2-yl	464	6.86	-0.43	1.33	5.10	8.54
2-388	F	7-bromo-1H-indol-6-yl	453	4.63	0.55	0.17	5.01	8.55
3-40	Cl	5-chloro-2-methylphenyl	400	-1.89	-0.50	-0.16	-2.55	9.98
3-51	Cl	3-chloro-2-(trifluorome-thyl)phenyl	454	9.26	0.19	-4.19	13.65	6.92
3-66	Cl	2.5-dimethylphenyl	380	9.92	-0.04	0.98	8.90	7.82
3-148	Cl	2- [4-(propan-2-yl)phenyl] ethyl	422	7.35	-0.30	4.14	2.90	8.95
3-311	Cl	7-fluoro-1*H*-inden-5-yl	408	2.78	1.08	-0.76	4.62	8.63
3-420	Cl	1-benzofuran-6-yl	392	1.15	0.15	1.41	-0.12	9.52
3-432	Cl	6-fluoro-2H-chromen-7-yl	424	-2.15	0.38	1.42	-3.18	10.10
4-257	Br	4.6-dimethylnaphthalen-2-yl	474	0.40	0.42	-0.16	0.98	9.32
4-378	Br	1H-indol-5-yl	435	0.14	2.59	0.78	1.95	9.13
4-424	Br	4-methyl-2*H*-chromen-7-yl	464	-1.52	0.03	-0.14	-1.35	9.76
4-434	Br	7-chloro-2H-chromen-2-yl	485	3.31	0.13	-1.03	4.47	8.66
5-81	I	2-chlorophenyl	478	3.61	0.23	-1.35	5.20	8.52
5-223	I	6-methoxypyrimidin-4-yl	475	8.45	-1.68	-0.25	7.02	8.17
5-399	I	6-methyl-2-benzofuran-5-yl	497	6.30	0.48	0.28	6.50	8.27
6-234	CH_3	4-methoxynaphthalen-2-yl	411	2.60	1.99	-0.78	5.37	8.49
6-269	CH_3	1,4-dimethylnaphthalen-2-yl	409	-2,50	-1,23	0,50	-4,23	10,30
6-444	CH_3	6-bromo-8a*H*-chromen-7-yl	464	1.42	0.07	0.35	1.14	9.29
6-496	CH_3	thianthren-2-yl	470	-4.91	4.99	-2.68	2.77	8.98
6-522	CH_3	1.4.5.8-tetramethylnaphtha-len-2-yl	438	-1.54	0.05	1.82	-3.31	10.13
7-109	C_2H_5	methyl 2-aminobenzoate	403	14.56	-0.32	-1.25	15.49	6.57
7-127	C_2H_5	2-(3-methylphenyl)ethyl	371	5.94	0.07	2.54	3.47	8.84
7-141	C_2H_5	2-(2-ethylphenyl)ethyl	385	11.56	-0.03	5.51	6.01	8.36
7-239	C_2H_5	3-bromonaphtalen-2-yl	474	8.48	-0.38	1.22	6.88	8.20
7-267	C_2H_5	5.8-dimethylnaphthalen-2-yl	423	-1.12	-3.24	5.97	-10.33	11.45

Designed analogs	Substituents		M_w [g.mol^{-1}]	$\Delta\Delta H_{MM}$ [kca.mol^{-1}]	$\Delta\Delta G_{sol}$ [kca.mol^{-1}]	$\Delta\Delta TS_{vib}$ [kca.mol^{-1}]	$\Delta\Delta G_{com}$ [kca.mol^{-1}]	pIC_{50}^{pred}
	R_1	R_2						
7-269	C_2H_5	1.4-dimethylnaphthalen-2-yl	423	3.84	-2.47	7.48	-6.11	10.65
7-270	C_2H_5	1.3-dimethylnaphthalen-2-yl	423	7.85	-1.98	6.21	-0.34	9.57
7-271	C_2H_5	naphthalen-1-yl	395	1.29	0.58	1.99	-0.11	9.52
7-272	C_2H_5	2-methylnaphthalen-1-yl	409	4.45	-0.16	2.75	1.54	9.21
7-273	C_2H_5	3-methylnaphthalen-1-yl	409	1.92	-0.30	4.03	-2.42	9.96
7-274	C_2H_5	4-methylnaphthalen-1-yl	409	0.40	0.88	2.03	-0.75	9.64
7-275	C_2H_5	5-methylnaphthalen-1-yl	409	0.67	1.33	-0.24	2.24	9.08
7-276	C_2H_5	6-methylnaphthalen-1-yl	409	1.27	0.58	2.95	-1.09	9.71
7-277	C_2H_5	7-methylnaphthalen-1-yl	409	0.73	1.14	-0.29	2.16	9.09
7-278	C_2H_5	8-methylnaphthalen-1-yl	409	5.39	-2.42	2.95	0.03	9.50
7-279	C_2H_5	2-chloronaphthalen-1-yl	430	-0.58	-0.62	2.00	-3.20	10.10
7-388	C_2H_5	7-bromo-1H-indol-6-yl	463	4.29	0.55	-0.93	5.76	8.41
7-522	C_2H_5	1.4.5.8-tetramethylnaphtha-len-2-yl	452	-0.32	-2.61	3.00	-5.93	10.62
7-524	C_2H_5	1.4.5.6.8-pentamethylnaph-thalen-2-yl	466	1.40	-3.53	6.69	-8.83	11.17
7-525	C_2H_5	1.4.5.7.8-pentamethylnaph-thalen-2-yl	466	1.80	-4.04	8.85	-11.09	11.60
7-526	C_2H_5	4.5.6.8-tetramethylnaphtha-len-2-yl	452	-1.01	-5.40	4.43	-10.85	11.55
8-20	isopropyl	3-tert-butylphenyl	416	10.60	-4.43	7.00	-0.83	9.66
8-30	isopropyl	4-methoxyphenyl	389	10.18	-1.90	1.90	6.38	8.29
8-315	isopropyl	1*H*-inden-6-yl	397	7.67	-0.60	0.85	6.22	8.32
8-331	isopropyl	2-methoxy-3H-inden-5-yl	427	-1.52	2.15	3.55	-2.91	10.05
8-332	isopropyl	3-methoxy-1H-inden-5-yl	427	2.96	-0.17	2.42	0.36	9.43
8-333	isopropyl	1-bromo-1H-inden-5-yl	476	1.51	-0.71	1.85	-1.05	9.70
8-334	isopropyl	7-bromo-1H-inden-5-yl	476	0.72	0.13	3.10	-2.25	9.93
8-335	isopropyl	6-bromo-1H-inden-5-yl	476	2.05	0.78	2.01	0.81	9.35
8-336	isopropyl	6-methoxy-1H-inden-5-yl	427	1.96	-0.04	2.75	-0.83	9.66
8-337	isopropyl	7-methoxy-1H-inden-5-yl	427	0.77	0.29	-3.53	4.59	8.63
8-338	isopropyl	1-methoxy-1H-inden-5-yl	427	1.23	-0.27	-1.48	2.43	9.04
8-339	isopropyl	2-methoxy-1H-inden-5-yl	427	-0.71	-0.07	-0.67	-0.12	9.52
8-353	isopropyl	4-methylpentalen-2-yl	397	7.87	-0.31	-0.43	7.99	7.99
8-361	isopropyl	1-hydroxyindol-6-yl	414	5.63	0.81	0.86	5.58	8.45
8-435	isopropyl	7-chloro-2H-chromen-3-yl	448	15.14	-1.34	3.91	9.88	7.63
8-468	isopropyl	5-chloro-2H-chromen-7-yl	448	5.44	0.91	-2.80	9.15	7.77
9-143	tert-butyl	2-(2-tert-butylphenyl)ethyl	458	40.60	3.77	8.68	35.70	2.75

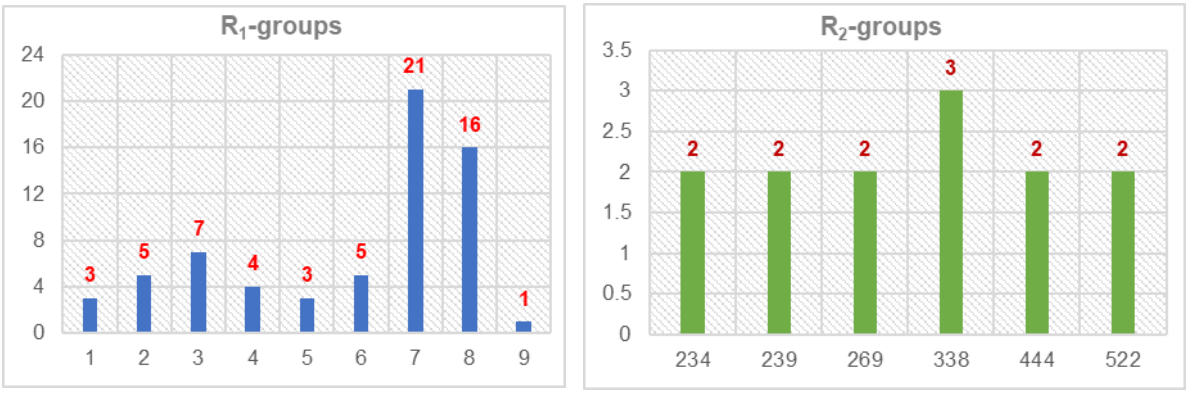

Figure 9. *Distribution histograms illustrating the occurrence rates of specific R-substituents among the top 65 analog hits that successfully align with four essential components of the Hypo1 pharmacophore model.*

Table 7. *In silico pharmacokinetic evaluation (ADME parameters) generated via QikProp for the most promising novel sulfonamides, benchmarked against established clinical and investigational anti-tuberculosis therapeutics [45].*

SULFx	HBdon	HBacc	$logP_{o/w}$	$logS_{wat}$	$logK_{HSA}$	BIP_{caco} [$nm.s^{-1}$]	#meta	IC_{50}^{Pred} [nM]	HOA	%HOA
7-525	2	9.5	2.4	-5.5	0.23	92	5	$2{,}51.10^{-3}$	3	76
7-526	2	9.5	2.7	-5.8	0.41	93	7	$2{,}81.10^{-3}$	2	78
7-269	2	9.5	1.9	-4.7	-0.01	95	3	$2{,}24.10^{-2}$	3	73
6-269	2	9.5	1.6	-4.6	-0.1	90	3	$5{,}01.10^{-2}$	3	71
Rifampicine	3	4.5	-0.7	0	-0.8	267.5	2	-	2	67
Isoniazid	2	5	-0.6	-0.5	-0.8	298.4	4	-	2	67
Ethambutol	4	6.4	-0.2	0.6	-0.8	107.8	4	-	2	62
Pyrazinamide	6	20.3 *	3.0	-3.1	-0.3	38.2	11 *	-	1	34
Gatifloxacin	1	6.8	0.5	-4.0	0	17.0	1	-	2	52
Moxifloxacin	1	6.8	1.0	-4.7	0.2	20.9	1	-	2	56
Rifapentine	6	20.9*	3.6	-2.2	-0.2	224.40	13	-	1	51
Bedaquiline	1	3.8	7.6*	-6.9	1.7	1562.2	5	-	1	100
Delamanid	0	6.0	5.8	-7.6	1.0	590.9	2	-	1	85
Linezolid	1	8.7	0.6	-2.0	-0.7	507.0	2	-	3	79
Sutezolid	1	7.5	1.3	-3.4	-0.4	449.3	0	-	3	82
Ofloxacin	0	7.3	-0.4	-2.8	-0.5	25.9	1	-	2	50
Amikacin	17*	26.9*	-7.9*	-0.2	-2.1	0	14*	-	1	0
Kanamycin	15*	227*	-6.7*	2.0	-1.4	0	12*	-	1	0
Imipenem	3	7.2	1.0	-1.8	-0.7	35.0	3	-	3	61
Amoxicillin	4,25	8.0	-2.5	-0.8	-1.1	1.0	5	-	1	12
Clavulanate	2	6.5	-0.8	0.3	-1.3	13.3	2	-	2	42

3.4. Structural and Thermodynamic Evaluation of the Novel Derivatives

The creation of the virtual library of new SULF derivatives was guided by an exploration of the structural diversity surrounding the active conformation of sulfonamides. To understand Structure-Activity Relationships (SAR) and identify the most promising inhibitors of the Eis enzyme, the substitution profiles at positions R1 and R2 were analyzed among the top 65 candidates from the virtual screening. The frequencies of occurrence of these different fragments (Figure 9), combined with their thermodynamic parameters (Table 5), highlight the main structural requirements associated with inhibitory activity. Statistical analysis of the fragment distribution reveals highly significant RSA trends. With regard to the R1 position, the data show a very strong preference for short aliphatic chains. Fragment F7 (ethyl) is by far the most prevalent with 21 occurrences, followed by fragment F8 (isopropyl, 16 occurrences). This high prevalence suggests that minimal steric hindrance at this position is critical for ensuring optimal spatial anchoring within the enzyme's binding pocket. Unlike position R1, position R2 appears to accommodate greater structural diversity, although specific motifs stand out clearly. The F338 fragment predominates with 3 occurrences, accompanied by a group of structurally related hydrophobic fragments such as F234, F239, F269, F444, and F522, each occurring twice. The recurrent selection of these bulky groups demonstrates the crucial importance of this position for maximizing affinity. These voluminous fragments most likely promote the formation of extensive hydrophobic interaction networks or π-stacking contacts with the aromatic residues lining the active site. The validity of this substitution profile is confirmed by the excellent scores of the best analogs identified. Analog 7-525, which effectively incorporates the F7 fragment into R1, stands out as the most promising candidate in the series with a $pIC_{50}^{pred} = 11.60$. This high inhibitory activity is corroborated by the remarkable thermodynamic stability of the enzyme-inhibitor complex ($\Delta\Delta G_{com} = -11.09\ kcal/mol$). Analogs 7-526 ($pIC_{50}^{pred} = 11.55$) and 7-267 ($pIC_{50}^{pred} = 11.45$) also validate this trend. In conclusion, these results show that the combination of a short alkyl group at R1 and a bulky hydrophobic moiety at R2 constitutes an optimal structural configuration for this scaffold. This arrangement could thus provide a rational framework for the development of future highly effective and highly specific inhibitors targeting the Eis enzyme.

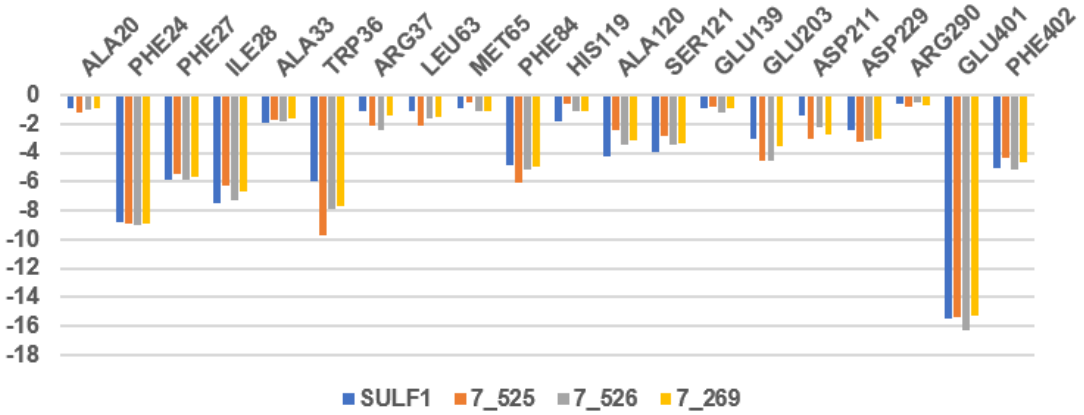

Figure 10. *Per-residue partitioning of the computed intermolecular interaction energies (E_{int} in kcal.mol^{-1}) comparing the three most favorable novel derivatives against SULF1, the reference high-affinity molecule from the TS. The color coding corresponds to the respective ligands.*

3.5. ADME Pharmacokinetic Profile of Designed Sulfonamide Analogs

Investigating the pharmacokinetic behavior of potential Eis blockers remains a critical step. As detailed in Table 7, the ADME characteristics of the newly formulated derivatives were evaluated in silico employing the QikProp algorithm, which relies on Jorgensen's established methodologies. To establish a reliable benchmark, the profiles of our leading candidates were evaluated alongside standard therapeutics currently utilized for tuberculosis management (Table 7).

3.6. Computational Molecular Dynamics Analysis

Computational MD assessments were conducted to study theses complexes. This approach allows for the analysis of structural stability over time (Figure 11). The initial complexes were derived from structures optimized by modeling. Each enzyme-ligand complex was analyzed individually. The simulations were performed using the Desmond software [34]. This program is well-suited for large biomolecular systems. The trajectories obtained describe the temporal evolution of the structures. The movements of the small molecule confined

inside the catalytic pocket were tracked. Overall structural robustness was assessed using RMSD values (Figure 13). These values provide information on conformational variations over time. The complexes exhibit limited fluctuations after equilibration. The ligands maintain a stable orientation within the enzyme cavity. Hydrophobic interactions remain dominant throughout the simulation. The observed hydrogen bonds persist for a significant duration. The solvent interacts regularly with exposed residues. These interactions contribute to the overall equilibrium of the system. The final conformations remain close to the initial structures. These observations confirm the stability of the studied complexes. The results support the relevance of the selected analogs (Figure 12).

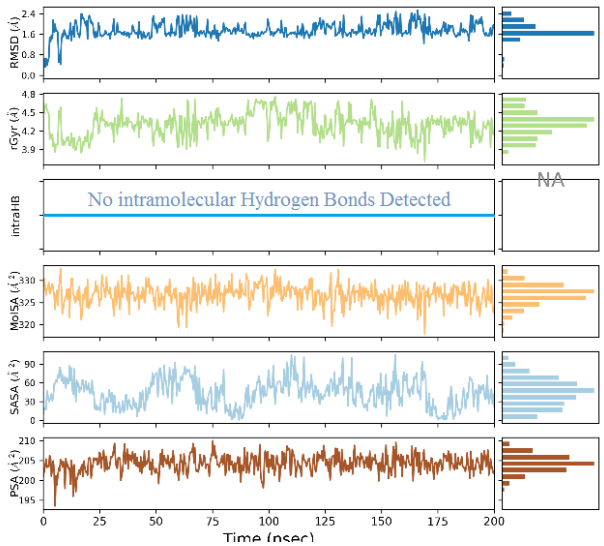

Sulfonamide 1

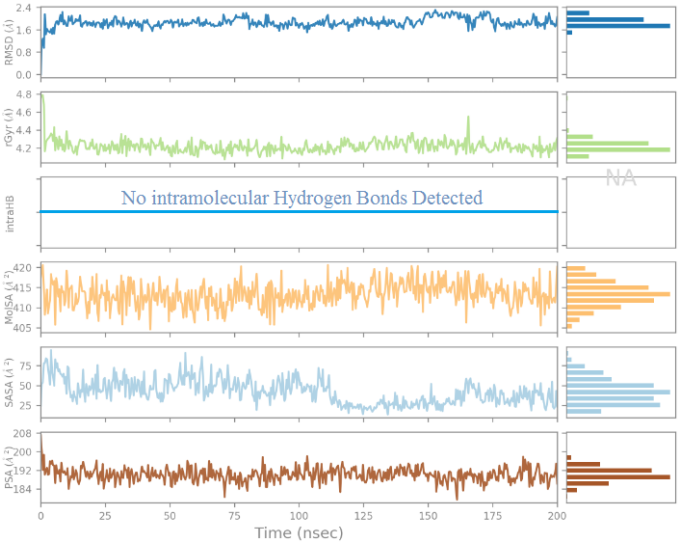

7-525

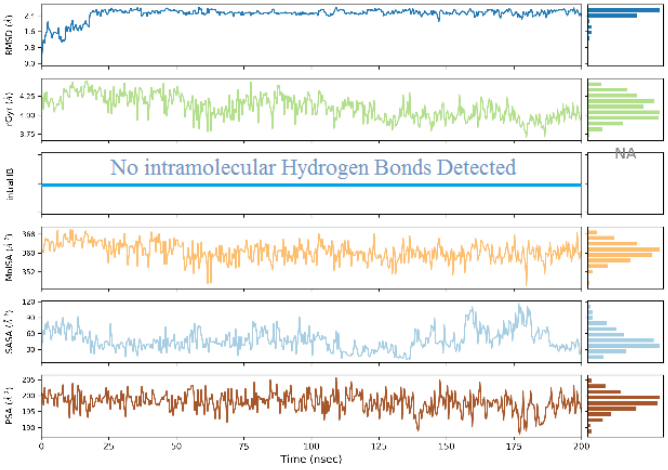

7-526

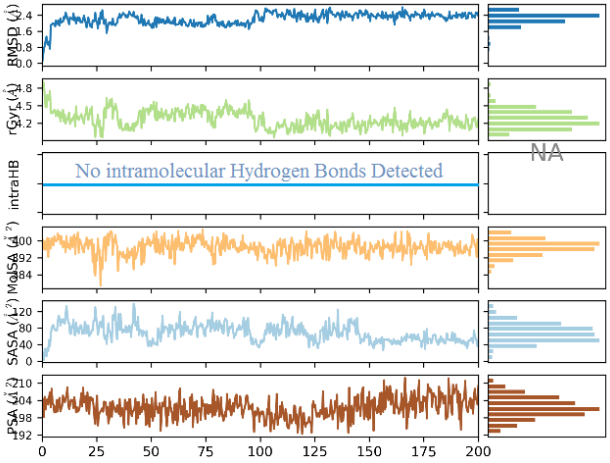

7-269

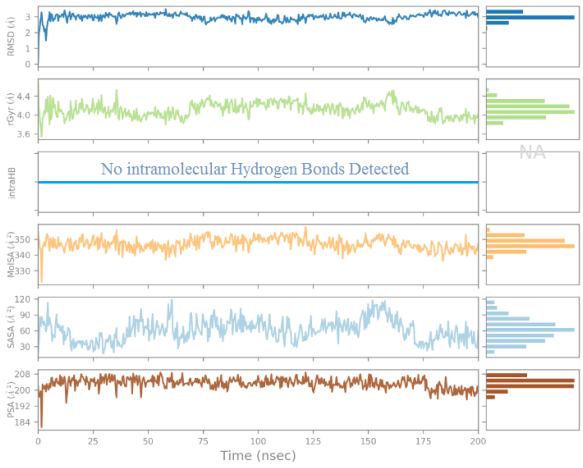

6-269

Figure 11. *Trajectory analysis depicting the temporal variation of SULF-Eis complex characteristics throughout 200 ns MD simulations. For each evaluated ligand, the graphs display the following parameters (from top to bottom) measured against the simulation timeframe: conformational root-mean-square deviation (RMSD) relative to the reference state, gyration radius (rGyr), internal hydrogen bond occurrences (intraHB), as well as the molecular (molSA), solvent-accessible (SASA), and polar (PSA) surface areas. Sulfonamide 1(SULF 1): the most active ligand among the molecules used in the training set.*

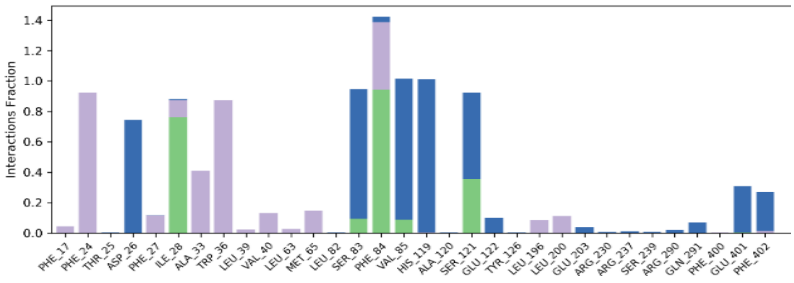

SULF1

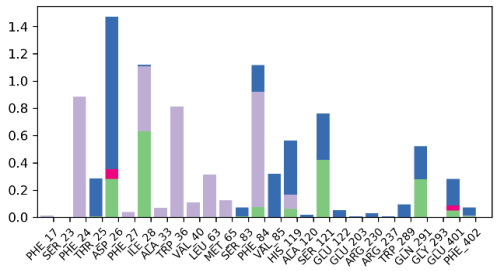

7-525

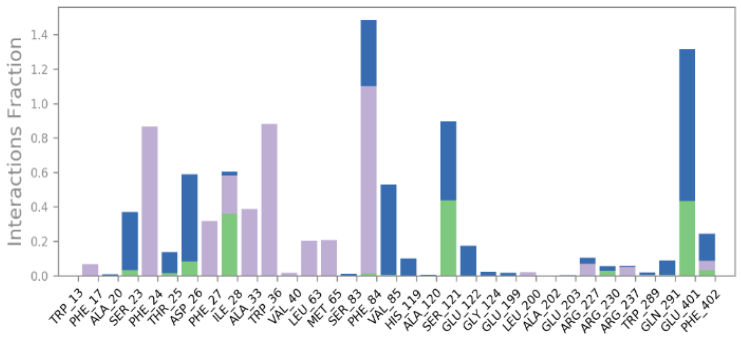

7-526

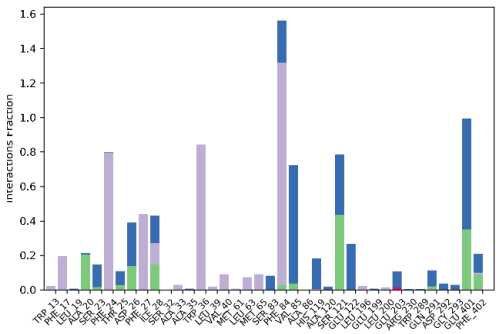

7-269

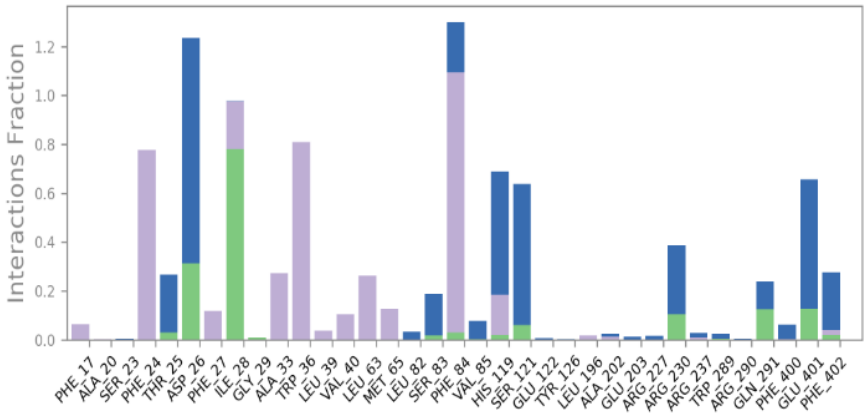

6-269

Figure 12. *Partitioning of specific catalytic pocket residue interactions involved in anchoring the inhibitors within the SULF-Eis systems over the course of MD trajectories. Interaction types are color-coded as follows: hydrogen bonds (green), ionic bonds (magenta), hydrophobic associations (purple), and water-mediated bridges (blue).*

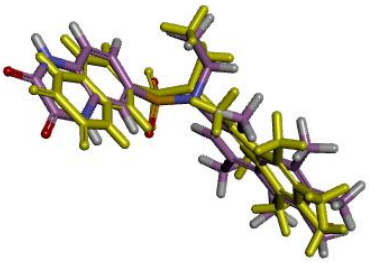

SULF 1 (RMSD: 2.12)

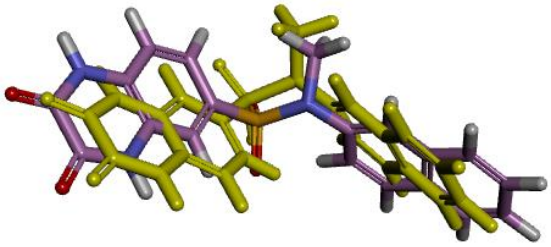

SULF 7-526 (RMSD: 1.01)

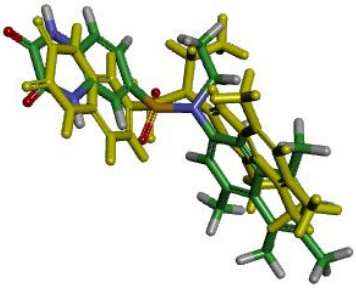

SULF 7-525 (RMSD: 2.31)

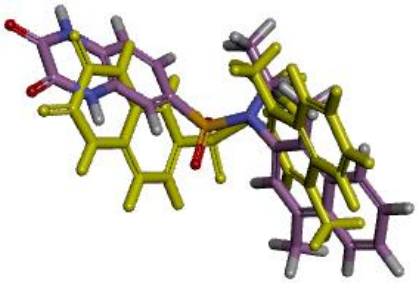

SULF 7-269 (RMSD: 2.25)

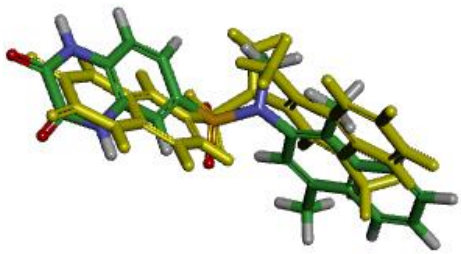

SULF 6-269 (RMSD: 2.57)

Figure 13. *Superimposition of the functionally active ligand geometries optimized via molecular mechanics against the mean operational conformations (depicted in gold) extracted from the molecular dynamics trajectories.*

3.7. MM-GBSA Thermodynamic Profiling of the Novel Eis Inhibitors

The relative binding free energies ($\Delta\Delta G_{MM-GBSA}$) were computed from the molecular dynamics simulation trajectories (Table 8) to assess the thermodynamic stability of the inhibitor-Eis complexes. Using the lead training set compound SULF1 as a reference, the ranking of the relative energies ($\Delta\Delta G_{MM-GBSA}$) is established as follows: SULF7-525 ($-17.62\ kcal/mol$) < SULF7-526 ($-15.30\ kcal/mol$) < SULF7-269 ($-11.14\ kcal/mol$) < SULF6-269 ($-4.28\ kcal/mol$). All newly designed analogues exhibit significantly more negative binding free energy values compared to the reference, highlighting a markedly more favorable interaction within the protein's active site. This affinity hierarchy is strictly maintained when analyzing the complexation relative free energies ($\Delta\Delta G_{comp}$), with values of -11.09, -10.85, -6.11, and -4.23 kcal/mol, respectively. It is worth noting a characteristic gap between the absolute magnitudes of $\Delta\Delta G_{MM-GBSA}$ and $\Delta\Delta G_{comp}$. Such discrepancies in amplitude are inherent to the distinct parametric approximations and force fields utilized by these two computational methods. However, the consistent ranking of the ligands across both approaches confirms the robustness of the scoring strategy employed. Moreover, the robust linear correspondence linking the calculated thermodynamic parameters to the anticipated in vitro potency provides highly convincing validation. Analogue SULF7-525, which displays the lowest binding energy, logically exhibits the highest inhibitory potential with a predicted IC_{50} (IC_{50}^{pred}) of 2.51 pM, closely followed by SULF7-526 with an estimated activity of 2.81 pM. These two lead candidates drastically outperform the reference molecule SULF1 (IC_{50}^{pred} of 240 pM), thereby validating the effectiveness of the structural modifications implemented in these new analogues.

Table 8. *Evaluation of the MM-GBSA thermodynamic binding parameters for the reference SULF1 and the optimized derivatives, extracted from the 200 ns molecular dynamics simulations.*

Inhibitors	Range $\Delta G(kcal.\ mol^{-1})$	Standard deviation $\Delta G(kcal.\ mol^{-1})$	MM-GBSA $\Delta G_{binding}(kcal.\ mol^{-1})$	$\Delta\Delta G_{MM-GBSA}$ $(kcal.\ mol^{-1})$	$\Delta\Delta G_{comp}$ $(kcal.\ mol^{-1})$	IC_{50}^{pred} (pM)
SULF1	-89.72 to -54.90	6.03	-70.4677	0.00	0.00	240
SULF7-525	-105.03 to -73.67	5.87	-88.0910	-17.6233	-11.09	2.51
SULF7-526	-110.87 to -57.10	8.78	-85.7695	-15.3018	-10.85	2.81
SULF7-269	-101.21 to -56.17	6.26	-81.6070	-11.1393	-6.11	22.4
SULF6-269	-104.06 to -45.58	8.44	-74.7527	-4.285	-4.23	50.1

4. Discussion

The results obtained show that the QSAR model developed exhibits good predictive robustness. Beyond its statistical performance, the structural analysis provides key insights. The specific binding networks formed between the SULF molecules and the Eis catalytic cavity elucidate the observed trends. Hydrophobic contacts play a central role in stabilizing the formed complexes. Aromatic interactions contribute significantly to the anchoring of ligands within the cavity. Additionally, London dispersion interactions play a critical role in optimizing the spatial arrangement within these complexes. Analysis of interaction energy highlights the involvement of major residues. The Trp36 and Phe84 residues contribute significantly to the stabilization of active ligands. These residues interact preferentially with bulky aromatic groups. The most potent ligands penetrate deeper into the hydrophobic pocket. This behavior is similar to that observed for compound 46 described previously. These observations confirm the importance of the hydrophobic region residing within the Eis enzymatic pocket. Evaluating the structural features of the various ligand categories inside the TS dataset reinforces this interpretation. Highly active inhibitors exhibit more favorable energy contributions. Weakly active ligands exhibit less stabilizing interactions. This trend confirms the relationship between energetic stabilization and inhibitory activity. It supports the validity of the QSAR model based on complexation energies. The most promising analogs identified through screening were studied in greater detail. The compounds SULF7-526, SULF7-525, SULF7-269, and SULF6-269 exhibit high activity. Their predicted inhibitory activities far exceed that of the reference compound. These ligands also exhibit very favorable interaction energy values. The consistency between QSAR predictions and energy trends validates the adopted strategy. Molecular dynamics simulations provide additional insight. They demonstrate good stability of

the complexes over time. The ligands maintain a stable orientation within the Eis active site. Hydrophobic interactions persist throughout the simulated trajectories. The observed hydrogen bonds reinforce the binding of the selected ligands. These results confirm the reliability of the conformations obtained through modeling. MM/GBSA calculations allow for a more realistic estimation of binding affinity. The average free energies confirm the superiority of the best analogs. These calculations incorporate solvent effects that are absent in static approaches. They reinforce the prioritization of the candidates identified by screening. Analysis of ADME properties completes the evaluation of the selected compounds. The best analogs exhibit profiles compatible with oral administration. No major concerns were detected for key pharmacokinetic parameters. These characteristics reinforce their potential as anti-tuberculosis candidates.

5. Conclusion

The current investigation relies upon the crystallographic coordinates characterizing the Eis enzyme bound to a sulfonamide. Specifically, the 5IV0 structure served as the basis for all modeling approaches. A reliable QSAR model was developed using the calculated complexation energies. This model shows a strong correlation with experimental inhibitory activities. A PH4 pharmacophore model was formulated utilizing the spatial geometries of the most potent derivatives. This model identified specific characteristics essential for inhibition. It served as a filter for screening a large virtual library. A selection based on ADME properties narrowed down the list of candidates. Sixty-five virtual analogs were identified as promising candidates. The QSAR model enabled the prediction of their relative inhibitory activities. Several compounds exhibit values significantly higher than the parent compound. The derivatives SULF7-526, SULF7-525, SULF7-269, and SULF6-269 stand out clearly. Computational MD trajectories further corroborate the structural robustness of these docked assemblies over time. MM/GBSA calculations reinforce the energetic assessment of their affinity. These approaches provide dynamic validation of the QSAR results. Overall, this study demonstrates the effectiveness of an integrated modeling strategy. The combination of QSAR, pharmacophore, molecular dynamics, and MM/GBSA is relevant. It enables the rational identification of new Eis inhibitors. These compounds represent serious candidates for future experimental studies. They open up prospects for overcoming kanamycin resistance.

Abbreviations

ADME	Absorption. Distribution. Metabolism. and Excretion
2D	Two-Dimensional
3D	Three-Dimensional
QSAR	Quantitative Structure-Activity Relationships
GFE	Gibbs Free Energy
VCL	Virtual Combinatorial Library
DHODH	Dihydroorotate Dehydrogenase
SULF	Sulfonamide
Eis	Enhance Intracellular Survival
IC_{50}^{exp}	Experimentally Half-Maximal Inhibitory Concentration
PH4	pharmacophore
WHO	World Health Organization
Mtb	Mycobacterium tuberculosis
VL	Virtual Library
TS	Test Set
VS	Validation Set
E-I	Enzyme-Inhibitor
Eint	Enzyme–Inhibitor Interaction Energy per Residue
$\Delta\Delta G_{com}$	Relative Complexation GFE
IC_{50}^{pred}	Predicted Half-Maximal Inhibitory Concentration
MD	Molecular Dynamics
MM	Molecular Mechanics
GBSA	Generalized Born Surface Area

Author Contributions

Bamba Ibrahim: Conceptualization, Methodology, Writing – original draft

Kouadja Rika Justin: Formal Analysis, Validation

Mousse Logbo Mathias: Project Administration, Resources, Supervision

Soro Issouf: Investigation, Software

Niare Adama: Data curation, Visualization

Megnassan Eugene: Writing – review & editing

Conflicts of Interest

The authors declare no conflicts of interest.

References

[1] World Health Organization. Global Tuberculosis Report 2025. Geneva: WHO; 2025.

[2] Dheda K, Gumbo T, Maartens G, Dooley KE, McNerney R, Murray M, et al. The epidemiology, pathogenesis, transmission, diagnosis, and management of multidrug-resistant, extensively drug-resistant, and incurable tuberculosis. Lancet Respir Med. 2017; 5(4): 291-360. https://doi.org/10.1016/S2213-2600(17)30079-6

[3] Gandhi NR, Nunn P, Dheda K, Schaaf HS, Zignol M, Van Soolingen D, et al. Multidrug-resistant and extensively drug-resistant tuberculosis: a threat to global control of tuberculosis. Lancet. 2010; 375(9728): 1830-1843. https://doi.org/10.1016/S0140-6736(10)60410-2

[4] Chen W, Biswas T, Porter VR, Tsodikov OV, Garneau-Tsodikova S. Unusual regioversatility of acetyltransferase Eis, a cause of drug resistance in XDR-TB. Proc Natl Acad Sci U S A. 2011; 108(24): 9815-9820. https://doi.org/10.1073/pnas.1105379108

[5] Willby MJ, Green KD, Gajadeera CS, Hou C, Tsodikov OV, Posey JE, Garneau-Tsodikova S. Potent Inhibitors of Acetyltransferase Eis Overcome Kanamycin Resistance in Mycobacterium tuberculosis. ACS Chem Biol. 2016; 11(6): 1639-1646. https://doi.org/10.1021/acschembio.6b00110

[6] Zaunbrecher MA, Sikes RD Jr, Metchock B, Shinnick TM, Posey JE. Overexpression of the chromosomally encoded aminoglycoside acetyltransferase Eis confers kanamycin resistance in Mycobacterium tuberculosis. Proc Natl Acad Sci U S A. 2009; 106(47): 20004-20009. https://doi.org/10.1073/pnas.0907925106

[7] Shin DM, Jeon BY, Lee HM, Jin HS, Yuk JM, Song CH, et al. Mycobacterium tuberculosis Eis regulates autophagy, inflammation, and cell death through redox-dependent signaling. PLoS Pathog. 2010; 6(12): e1001230. https://doi.org/10.1371/journal.ppat.1001230

[8] Jennings BC, Labby KJ, Green KD, Garneau-Tsodikova S. Redesign of substrate specificity and identification of the aminoglycoside binding residues of Eis from Mycobacterium tuberculosis. Biochemistry. 2013; 52: 5125-5132. https://doi.org/10.1021/bi4002985

[9] Punetha A, Ngo HX, Holbrook SYL, Green KD, Willby MJ, Bonnett SA, et al. Structure-Guided Optimization of Inhibitors of Acetyltransferase Eis from Mycobacterium tuberculosis. ACS Chem Biol. 2020; 15(6): 1581-1594. https://doi.org/10.1021/acschembio.0c00184

[10] Houghton JL, Biswas T, Chen W, Tsodikov OV, Garneau-Tsodikova S. Chemical and structural insights into the regioversatility of the aminoglycoside acetyltransferase Eis. ChemBioChem. 2013; 14: 2127-2135. https://doi.org/10.1002/cbic.201300359

[11] Ovung A, Bhattacharyya J. Sulfonamide drugs: structure, antibacterial property, toxicity, and biophysical interactions. Biophys Rev. 2021; 13(2): 259-272. https://doi.org/10.1007/s12551-021-00795-9

[12] Kitchen DB, Decornez H, Furr JR, Bajorath J. Docking and scoring in virtual screening for drug discovery: methods and applications. Nat Rev Drug Discov. 2004; 3: 935-949. https://doi.org/10.1038/nrd1549

[13] Roy K, Kar S, Das RN. A Primer on QSAR/QSPR Modeling. Springer; 2015.

[14] Hollingsworth SA, Dror RO. Molecular dynamics simulation for all. Neuron. 2018; 99(6): 1129-1143. https://doi.org/10.1016/j.neuron.2018.08.011

[15] Hou T, Wang J, Li Y, Wang W. Assessing the performance of MM/PBSA and MM/GBSA methods. J Chem Inf Model. 2011; 51(1): 69-82. https://doi.org/10.1021/ci100275a

[16] Conradie F, Diacon AH, Ngubane N, et al. Treatment of highly drug-resistant pulmonary tuberculosis. N Engl J Med. 2020; 382: 893-902. https://doi.org/10.1056/NEJMoa1901814

[17] Garzan A, Willby MJ, Green KD, et al. Sulfonamide-based inhibitors of Eis abolish kanamycin resistance in Mycobacterium tuberculosis. ACS Infect Dis. 2016; 2(6): 423-430. https://doi.org/10.1021/acs.jmedchem.6b01161

[18] OECD. Guidance Document on the Validation of (Quantitative) Structure-Activity Relationship [(Q)SAR] Models; OECD Series on Testing and Assessment, No. 69; OECD Publishing: Paris, France, 2014.

[19] Insight-II and Discover Molecular Modeling and Simulation Package, version 2005; Accelrys: San Diego, CA, USA, 2005.

[20] Discovery Studio molecular modeling and simulation program, Version 2.5, Accelrys, Inc., San Diego, CA, 2009.

[21] Niar é A, Alex AYZ, Bernard DAM, Marius KS, St éphane DS, Moise KA, Guy-Richard KM, Fagnidi YKH, Doh S. Study by molecular docking of the interactions between dihydroorotate dehydrogenase and a series of inhibitors of pyrrole derivatives for the treatment of malaria. Asian Journal of Chemical Sciences. 2025; 15(1): 92-110.

[22] Soro I, N'Guessan H, Abou A, N'Guessan RK, Megnassan E. Conformational study of molecules in a biological environment, design of inhibitors of human aminopeptidase M1 implicated in cancer therapy. Universal J Pharm Res. 2023; 8(5): 71-86. https://doi.org/10.22270/ujpr.v8i5.1011

[23] Kouadja RJ, Mousse LM, Kouman KC, Nsangou M, Megnassan E. Computer-assisted design of benzoisoxazol derivatives inhibitors of bromodomain-containing protein 4 (BRD4) with favorable pharmacokinetic profile. Int J Pharm Sci Drug Res. 2023; 15(5): 647-664. https://doi.org/10.25004/IJPSDR.2023.150514

[24] Niar é A, N'Guessan H, Dali B, Megnassan E. Computer-assisted design of hydroxamic acid derivatives inhibitors of M1 metallo aminopeptidase of Plasmodium falciparum with favorable pharmacokinetic profile. J Pharm Res Int. 2022; 34(60): 21-44. https://doi.org/10.9734/JPRI/2022/v34i607271

[25] Maple JR, Hwang M, Stockfisch TP, Dinur U, Waldman M, Ewig CS, Hagler AT. Derivation of class II force fields. I. Methodology and quantum force field for the alkyl functional group and alkane molecules. J Comput Chem. 1994; 15: 162-182. https://doi.org/10.1002/jcc.540150207

[26] Bieri C, Esmel A, Keita M, Owono LCO, Dali B, Megnassan E, Miertus S, Frecer V. Structure-Based Design and Pharmacophore-Based Virtual Screening of Combinatorial Library of Triclosan Analogs Active against Enoyl-Acyl Carrier Protein Reductase of Plasmodium falciparum with Favourable ADME Profiles. Int J Mol Sci. 2023; 24: 6916. https://doi.org/10.3390/ijms24086916

[27] Gilson MK, Barry HH. The inclusion of electrostatic hydration energies in molecular mechanics calculations. J Comput Aided Mol Des. 1991; 5(1): 5-20. https://doi.org/10.1007/BF00173467

[28] Miertuš S, Scrocco E, Tomasi J. Electrostatic interaction of a solute with a continuum. A direct utilization of ab initio molecular potentials for the prevision of solvent effects. Chem Phys. 1981; 55: 117-129. https://doi.org/10.1016/0301-0104(81)85090-2

[29] Niaré A, N'Guessan A-B, Djako BA, Dembélé GS, Koné MG-R, Yéo Y. QSAR, pharmacophore, and molecular docking studies for the design of novel arylamide-derived inhibitors of Mycobacterium tuberculosis. Chemical Science International Journal. 2024; 33(6): 212-224.

[30] Fischer S, Smith JC, Verma CS. Dissecting the vibrational entropy change on protein/ligand binding: Burial of a water molecule in bovine pancreatic trypsin inhibitor. J Phys Chem B. 2001; 105: 8050-8055. https://doi.org/10.1021/jp0120920

[31] Fofana I, Dali B, Koné M, Sujova K, Megnassan E, Miertus S, Frecer V. In Silico Optimization of Inhibitors of the 3-Chymotrypsin-like Protease of SARS-CoV-2. Life. 2025; 16(1): 6.

[32] Wienen-Schmidt B, Jonker HR, Wulsdorf T, Gerber HD, Saxena K, Kudlinzki D, Klebe G. Paradoxically, most flexible ligand binds most entropy-favored: intriguing impact of ligand flexibility and solvation on drug-kinase binding. J Med Chem. 2018; 61(14): 5922-5933.

[33] QikProp; Version 3.7, Release 14, X Schrödinger; LLC: New York, NY, USA, 2014.

[34] Desmond Molecular Dynamics System. Release 2021-2; Schrödinger LLC: New York, NY, USA, 2021.

[35] Frecer V, Miertus S. Antiviral agents against COVID-19: Structure-based design of specific peptidomimetic inhibitors of SARS-CoV-2 main protease. RSC Adv. 2020; 10: 40244-40263. https://doi.org/10.1039/D0RA08304F

[36] Wang X, Xu Y, Zheng H, Yu K. An Extendible, Graph-Neural-Network-Based Approach for Accurate Force Field Development of Large Flexible Organic Molecules. arXiv preprint arXiv: 2106.00927. 2021. https://doi.org/10.48550/arXiv.2106.00927

[37] Herbert JM. Dielectric continuum methods for quantum chemistry. WIREs Comput Mol Sci. 2022; 12(1): e1519. https://doi.org/10.1002/wcms.1519

[38] Kansal N, Silakari O, Ravikumar M. Three dimensional pharmacophore modelling for c-Kit receptor tyrosine kinase inhibitors. Eur J Med Chem. 2010; 45(1): 393-404.

[39] Barber C, Heghes C, Johnston L. A framework to support the application of the OECD guidance documents on (Q) SAR model validation and prediction assessment for regulatory decisions. Comput Toxicol. 2024; 30: 100305.

[40] N'Guessan H, Soro I, Keita M, Megnassan E. Design and In silico Screening of Combinatorial Library of New Herbicidal Analogs of Cycloalka [d] quinazoline2, 4dione-Benzoxazinones Inhibiting Protoporphyrinogen IX Oxidase. J Pharm Res Int. 2022; 34(56): 42-61.

[41] Keita M, Yaya Y, Yvon BMB, Esmel AE, Dali B, N'Guessan H. Molecular and Thermodynamic Modeling of the Protein-Ligand Interaction. Application to Computer-Assisted Design of Anti-Competitive Inhibitors of Human Histone Deacetylase. 2021; 2: 606-630. https://doi.org/10.25177/JCCMM.5.2.RA.10763

[42] Adama N, N'Guessan H, Dali B, Megnassan E. Computer-assisted design of hydroxamic acid derivatives inhibitors of M1 Metallo Aminopeptidase of Plasmodium falciparum with favorable pharmacokinetic profile. J Pharm Res Int. 2022; 21-44. https://doi.org/10.9734/jpri/2022/v34i607271

[43] Revillo Imbernon J, Jacquemard C, Bret G, Marcou G, Kellenberger E. Comprehensive analysis of commercial fragment libraries. RSC Med Chem. 2022; 13(3): 300-310. https://doi.org/10.1039/D1MD00363A

[44] Davis JM, Smith LR. Advances in computational approaches for estimating passive permeability in drug discovery. Membranes. 2023; 13(11): 851. https://doi.org/10.3390/membranes13110851

[45] QikProp 6.5. Release 139; Schrödinger LLC.: New York, NY, USA, 2019.